J. Fluid Mech. (2003), *vol.* 478, *pp.* 71–80.
DOI: 10.1017/S0022112002003038 Printed in the United Kingdom

The viscous catenary

By J. TEICHMAN AND L. MAHADEVAN†

Hatsopoulos Microfluids Laboratory, Massachusetts Institute of Technology, 77 Massachusetts Avenue, Cambridge, MA 02139, USA

(Received 29 September 2002 and in revised form 21 October 2002)

A filament of an incompressible highly viscous fluid that is supported at its ends sags under the influence of gravity. Its instantaneous shape resembles that of a catenary, but evolves with time. At short times, the shape is dominated by bending deformations. At intermediate times, the effects of stretching become dominant everywhere except near the clamping boundaries where bending boundary layers persist. Finally, the filament breaks off in finite time via strain localization and pinch-off.

1. Introduction

In 1690, Jacob Bernoulli issued the following challenge: determine the shape of a heavy filament or chain hanging between two points on the same horizontal line. Leibniz, Huygens and Johann Bernoulli independently discovered the equation for the shape of the catenary (derived from the Latin for chain), providing one of the first exact solutions of a nonlinear problem in continuum mechanics. Here we consider the fluid analogue of a catenary, shown in figure 1(*a–f*). When a thin filament of an incompressible highly viscous fluid forms a bridge across the gap between two solid vertical walls, it will sag under the influence of gravity. After a very short initial transient when it falls quickly, it slows down in response to the resistance to extension. During this process, it starts to thin, and thus speeds up, albeit inhomogeneously, eventually leading to necking and pinch-off, even in the absence of interfacial tension. The richness of this problem is paradigmatic of the free-boundary problems that are common in materials processing in such instances as filament spinning, glass manufacture etc. In addition the problem illustrates an application, to geometrically nonlinear problems, of the classical analogy between the equations of equilibrium for a linear elastic (Hookean) solid and the equations of motion for the creeping flow of a (Newtonian) fluid, due to Stokes (1845) and Rayleigh (1922).

2. Equations of motion

Consider an axisymmetric filament that is initially horizontal with the arc-length coordinate s denoting the centreline of the unstretched filament. As it starts to sag (figure 2), the filament starts to bend and stretch and the centreline has an arc-length $\bar{s}(s,t)$. The kinematic variables of interest are the angle of the tangent to the centreline with the horizontal $\theta(s,t)$, the vertical displacement of the centreline $H(s,t)$, the cross-sectional area $A(s,t) = \pi h^2/4$, where $h(s,t)$ is the filament diameter, and the local filament stretch $\lambda(s,t) = \partial\bar{s}/\partial s$. The dynamical variables of interest are the tangential

† Present address: Department of Applied Mathematics and Theoretical Physics, University of Cambridge, Centre for Mathematical Sciences, Wilberforce Road, Cambridge CB3 0WA, UK.

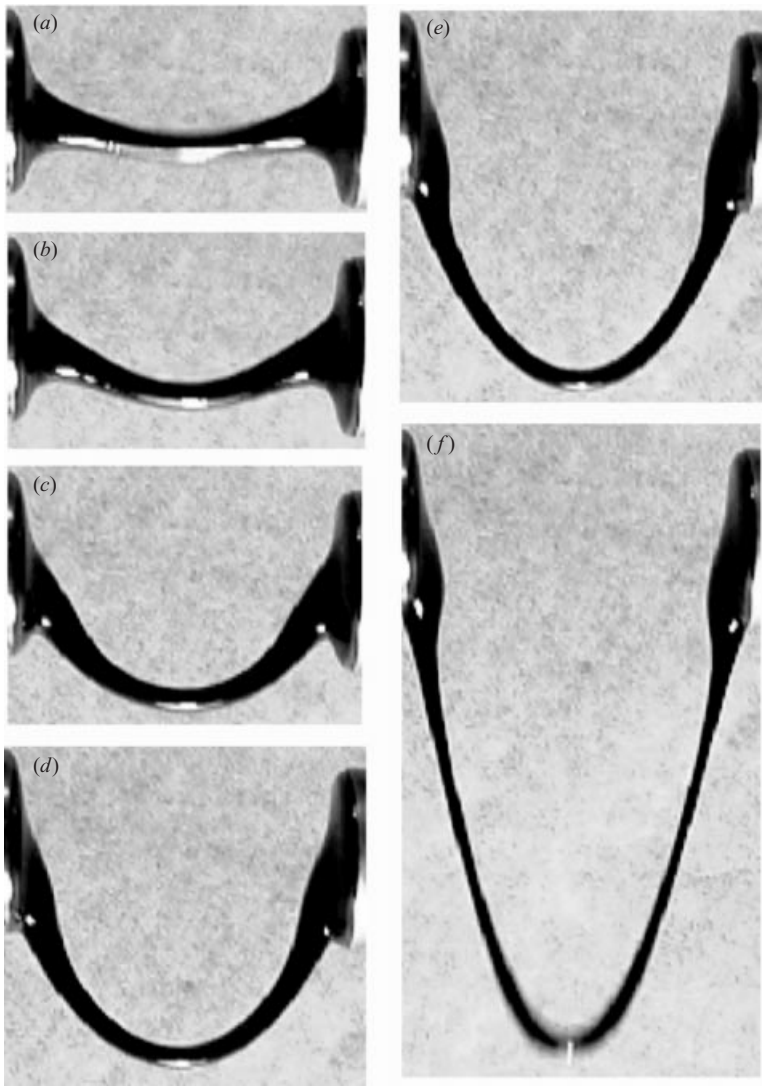

FIGURE 1. Snapshots of a filament of Lyle's golden syrup, dyed with carbon black, of initial diameter 3 mm and initial length 2 cm as it sags under its own weight at time (*a*) $t = 0+$, (*b*) $t = 0.04$ s, (*c*) $t = 0.64$ s, (*d*) $t = 1.24$ s, (*e*) $t = 1.84$ s, (*f*) $t = 2.44$ s. The viscosity of the liquid $\mu \approx 20$ Pa s, the density $\rho \approx 10^3$ kg m^{-3}, and the surface tension $\sigma \approx 30 \times 10^{-3}$ mN m^{-1}. The capillary number $\mu U/\sigma \geqslant 10$, so that we can neglect the effect of surface tension over the course of events depicted here.

stress resultant (tension) $T(s,t)$, the normal (shear) stress resultant $N(s,t)$, and the torque resultant $M(s,t)$. Assuming that the sagging always occurs sufficiently slowly that inertia may be neglected, the equations for the balance of forces and torques may be written as (Love 1944)

$$T_s - N\theta_s - w\sin\theta = 0, \tag{2.1}$$

$$N_s + T\theta_s - w\cos\theta = 0, \tag{2.2}$$

$$M_s + N = 0. \tag{2.3}$$

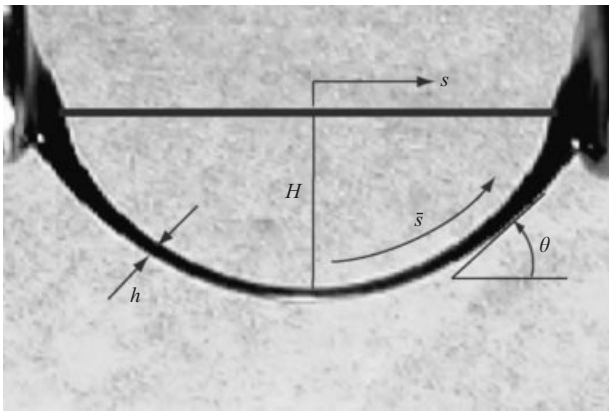

FIGURE 2. Schematic of the viscous catenary (not to scale) showing the notation.

Here and elsewhere $(a)_b \equiv \partial a/\partial b$, $w = \rho g A(x,0) \equiv \rho g A_0$ is the weight per unit length of the undeformed filament, and we have assumed that the only body forces are due to gravity. These equations make no reference to the constituent material of the filament; indeed, they are not closed as posed. Here, we have assumed that the interfaces are traction-free.

For the classical catenary, closure is brought about by using the constraint of inextensibility $s = \bar{s}$ and the requirement that the chain cannot support bending moments, i.e. $M = 0$. Then $T_s = w\sin\theta$, $T\theta_s = w\cos\theta$, where s is the arc-length coordinate that describes the inextensible chain. Solving these differential equations gives $\tan\theta = ws/T(0)$ and thus the shape

$$H(x) = H(0) + \frac{T(0)}{w}\left(\cosh\left(\frac{wx}{T(0)}\right) - 1\right).$$

When the length of the catenary is not much larger than the distance between the supports, $\theta \ll 1$, so that $s \approx x$, and $H(x) = H(0) + wx^2/T(0)$, which limit will be the focus of much of this paper.

For a filament of Newtonian fluid, continuity and the closure relations read

$$(A\lambda)_t = 0, \tag{2.4}$$

$$T = 3\mu A(\ln\lambda)_t, \tag{2.5}$$

$$M = D\theta_{st}, \tag{2.6}$$

where $D = 3\mu\pi h^4/64 = 3\mu A^2/4\pi$ is the bending stiffness of the filament. This law is a simple generalization of the constitutive equation for the bending of an elastic beam, where $M = 3\mu_e\pi h^4\theta_s/64$, with μ_e the shear modulus of the material, and follows directly from the Stokes–Rayleigh analogy (Stokes 1845; Rayleigh 1922; Taylor 1969; Johnson & Fletcher 1994; Mahadevan, Ryu & Samuel 1998; da Silveira, Chaieb & Mahadevan 2000; Skorobogatiy & Mahadevan 2000). We note that this presumes that the interfacial forces due to surface tension γ are dominated by viscous forces, i.e. the capillary number $Ca = \mu U/\gamma \gg 1$. Furthermore, here we have used a Lagrangian description convenient in the analysis of finite deformations (and their rates). Combining (2.1), (2.2), (2.3) and (2.6) to eliminate T, N and M we obtain

$$D\left(\left(\frac{\theta_{ssst}}{\theta_s}\right)_s + \theta_s\theta_{sst}\right) - w\left(2\sin\theta + \frac{\theta_{ss}\cos\theta}{\theta_s^2}\right) = 0. \tag{2.7}$$

Multiplying (2.7) by $\cos\theta$ and integrating the resulting equation yields

$$D\left(\frac{\theta_{ssst}\cos\theta}{\theta_s}+\theta_{sst}\sin\theta\right)+\frac{w\cos^2\theta}{\theta_s}=f_1(t), \tag{2.8}$$

where $f_1(t)$ is a constant of integration. Substituting $\theta=0$ into (2.8) and comparing the result with (2.2) yields $f_1(t)=T(0,t)$, the tension at the mid-point of the catenary. Multiplying (2.8) by $\theta_s/\cos^2\theta$ and integrating yet again gives

$$D\theta_{sst}\sec\theta+ws=T(0,t)\tan\theta+f_2(t), \tag{2.9}$$

where $f_1(t)$ is a constant of integration. Symmetry dictates that $\theta(0,t)=\theta_{sst}(0,t)=0$, so that $f_2(t)=0$. The boundary conditions that complete the formulation of the problem are

$$\theta(0,t)=0, \quad \theta(\pm L/2,t)=0. \tag{2.10}$$

For small to moderate deflections, when $\theta<1$, $s\approx x$ so that $H_x\approx\theta$, $\lambda\approx 1+u_x+H_x^2/2$, where $u(x,t)$ is the horizontal displacement of a cross-sectional element at location x. Then equations (2.1)–(2.9) simplify to

$$A=A_0, \tag{2.11}$$

$$T(x,t)=3\mu A(V_x+H_xH_{xt}), \tag{2.12}$$

$$T_x=0, \tag{2.13}$$

$$DH_{xxxxt}=TH_{xx}-w. \tag{2.14}$$

Here $V(x,t)=u_t$ is the horizontal component of the centreline velocity while H_t is the vertical component of the centreline velocity, so the extensional strain rate is $(\ln\lambda)_t\approx V_x+(H_x^2/2)_t$. We note that (2.11)–(2.14) are analogous to the Föppl–von Kármán equations for the bending and stretching of an elastic filament or sheet (Love 1944; Howell 1996), consistent with the Stokes–Rayleigh analogy. Using (2.13), the boundary condition $V(\pm L/2,t)=0$ and the symmetry of the problem which leads to $V(0,t)=0$, we can integrate (2.12) so that

$$\int_0^{L/2}T(t)\,\mathrm{d}x=L/2\,T(t)=3\mu A\int_0^{L/2}(H_x^2)_t\,\mathrm{d}x,$$

i.e. the average tension arises solely from the stretching induced by the bending deformations of the filament. Substituting the result into the integrated form of (2.14) yields a nonlinear integro-differential equation for $\theta(x,t)$:

$$D\theta_{xxt}-\frac{3\mu A}{L}\theta\int_0^{L/2}(\theta^2)_t\,\mathrm{d}x=-wx \tag{2.15}$$

subject to the boundary conditions (2.10). Next, we rescale all lengths by the initial length L of the filament, and time by a characteristic time $3\pi\mu h/2w$ determined by the balance between gravity and viscosity. Then, on defining $\epsilon=h/L$, we may write a dimensionless form of (2.15) and (2.10) as

$$\left.\begin{aligned}\epsilon^3\frac{\theta_{xxt}}{32}-\epsilon\frac{\theta}{2}\int_0^{1/2}(\theta^2)_t\,\mathrm{d}x=-x,\\ \theta(0,t)=\theta(\pm 1/2,t)=0.\end{aligned}\right\} \tag{2.16}$$

The first term in (2.16) represents the resistance to viscous bending; the second term represents the resistance to viscous stretching; and the inhomogeneous forcing term arises from the weight of the filament. Since $\epsilon \ll 1$, we see that the resistance to bending is far smaller than the resistance to stretching, as expected.

3. Early-time behaviour

During the early stages of the sagging of the filament, $\theta \ll 1$, in which case (2.16) may be further simplified to

$$\frac{\epsilon^3}{32}\theta_{xxt} = -x. \tag{3.1}$$

Integrating (3.1) with the initial condition $\theta(x,0) = 0$ and the boundary conditions (2.10) and $H(L/2,t) = 0$, yields

$$\left.\begin{aligned} \theta(x,t) &= -\frac{16\epsilon^{-3}x^3t}{3} + \frac{4\epsilon^{-3}xt}{3}, \\ H(x,t) &= \int_{-1/2}^{x} \theta \,\mathrm{d}x = -\frac{4\epsilon^{-3}t}{3}[\tfrac{1}{4} - x^2]^2. \end{aligned}\right\} \tag{3.2}$$

In dimensional terms,

$$\theta(x,t) = -\frac{wx^3t}{6D} + \frac{wL^2xt}{24D}, H(x,t) = -\frac{wt}{24D}\left[\left(\frac{L}{2}\right)^2 - x^2\right]^2.$$

This solution describes the sagging of a viscous filament at short times (Trouton 1906) in exact analogy with the sagging of an elastic filament of bending stiffness $D_e = D/t$ valid for small strains. As time progresses, the filament begins to stretch; we cannot neglect the resistance due to stretching even though there is but a small variation in the diameter because although $A_t \to 0$, $\mu \to \infty$, $T = -3\mu A_t$ remains finite.

After a time t, the tension in the filament scales as $T(t) \sim \mu h^2 (H_x^2)_t \sim \mu h^4/L^2 t$, so that the normal force generated per unit length in the curved filament is $TH_{xx} \sim \mu h^5/L^4 t$. Balancing this against the specific weight of the filament yields a critical time $t_c \sim \mu h^5/wL^4$ beyond which stretching effects can no longer be ignored. For the filament shown in figure 1, $L \sim 0.02\,\mathrm{m}$, $h \sim 0.003\,\mathrm{m}$, $\mu \sim 20\,\mathrm{Pa\,s}$, $\rho \sim 10^3\,\mathrm{kg\,m^{-3}}$, $t_c \sim 10^{-7}\,\mathrm{s}$! For comparison, the time t_S required for the development of Stokes layers that allow the influence of the wall to be felt in the interior of the filament scales as $h^2\rho/\mu$. Substituting typical parameter values associated with golden syrup, we find that $t_S \sim 10^{-1}\,\mathrm{s}$, i.e. the bending solution is difficult to observe in practice unless the fluid viscosity is large enough and the Stokes layer develops relatively fast. Thus, the pure bending regime is too brief to be visible in the sequence shown in figure 1; however, for thicker filaments of higher viscosity this effect should be clearly visible. In figure 3, we show the evolution of the shape of the catenary in and slightly beyond the bending-dominated regime. For comparison, we also show the result obtained by solving the complete system (2.16) numerically by using a spectral collocation method with Chebyshev-polynomial basis functions. We see that the bending solution which neglects the resistance to extension of the centreline over-estimates the sag of the filament, as expected.

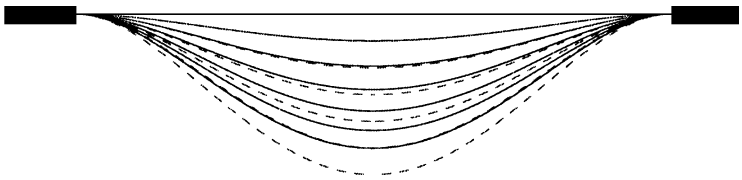

FIGURE 3. The evolution of the filament height $H(x,t) = \int_{-1/2}^{x} \theta(x,t)\,\mathrm{d}x$ as a function of time. Here the aspect ratio of the filament $\epsilon = 0.02$, and its scaled initial length is unity. The vertical deformation is amplified by a factor of 10 for ease of visualization. At short times, the filament deforms primarily by bending, with the maximum sag $|H(0,t)| \sim t$. The dashed line corresponds to the bending solution given by (3.2), while the solid line arises from a numerical solution to (2.16).

4. Intermediate-time behaviour

When $t > t_c$, the effects of bending, which hitherto were significant over the entire length of the filament, become localized to a $\delta(\epsilon,t)$ neighbourhood of the lateral attachment boundaries, while elsewhere the filament is subject primarily to extensional strains that do not vary locally over a cross-section. Thus, over most of the filament we have a balance between stretching and gravity for the 'outer' solution $\theta^{(o)}(x,t)$ which satisfies

$$\epsilon\theta^{(o)} \int_0^{L/2} (\theta^{(o)^2})_t \,\mathrm{d}x = 2x, \tag{4.1}$$

and has the exact solution

$$\theta^{(o)} = 72^{1/3}\epsilon^{-1/3} x t^{1/3}, \qquad x \in [0, L/2 - \delta]. \tag{4.2}$$

In dimensional terms $\theta^{(o)} = (12w/\mu A L^2)^{1/3} x t^{1/3}$. Substituting in parameter values for the filament shown in figure 1, we find that $H(0,t)/L \sim (12w/\mu A L^2)^{1/3} L t^{1/3}$, so that for $t \sim 1$ s, we obtain $H(0,t)/L \sim 10$, in good qualitative agreement with observations. The filament now sags much more slowly than in the bending regime, due to the increased resistance to stretching, as can be seen from the sequence of images in figure 1(b–e).

In figure 4, we show the evolution of the catenary shape in this intermediate regime; for comparison both the outer solution (4.2) and the numerical solution to (2.16) are shown. As time evolves, we see that, apart from a constant that arises from the difference between the initial bending transient, the difference between them is limited to a small neighbourhood of the lateral attachment regions. The lateral extent of these bending boundary layers decreases with time, so that (4.2) becomes an increasingly accurate approximation of the shape of the catenary.

In this boundary layer, where the filament must be highly curved, the outer solution must change rapidly to match the condition $\theta(\pm 1/2) = 0$. Balancing the bending term in (2.16) $\epsilon^3\theta_{xxt} \sim \epsilon^3\theta^{(o)}/\delta^2 t \sim \epsilon^{8/3} x t^{-2/3}\delta^{-2}$ with the weight x yields the width $\delta(\epsilon,t)$ of the bending boundary layer as

$$\delta \sim \epsilon^{4/3} t^{-1/3}. \tag{4.3}$$

In dimensional terms, $\delta \sim (\mu h^5/wL)^{1/3} t^{-1/3}$. This is the viscous analogue of the elastic boundary layer near the clamped boundary in a catenary with a small bending stiffness, where $\delta \sim (\mu_e h^5/wL)^{1/3}$, with μ_e being the shear modulus of the material of the catenary. In figure 5(a–c), we show that the results of numerical simulations of (2.16) confirming the above scaling.

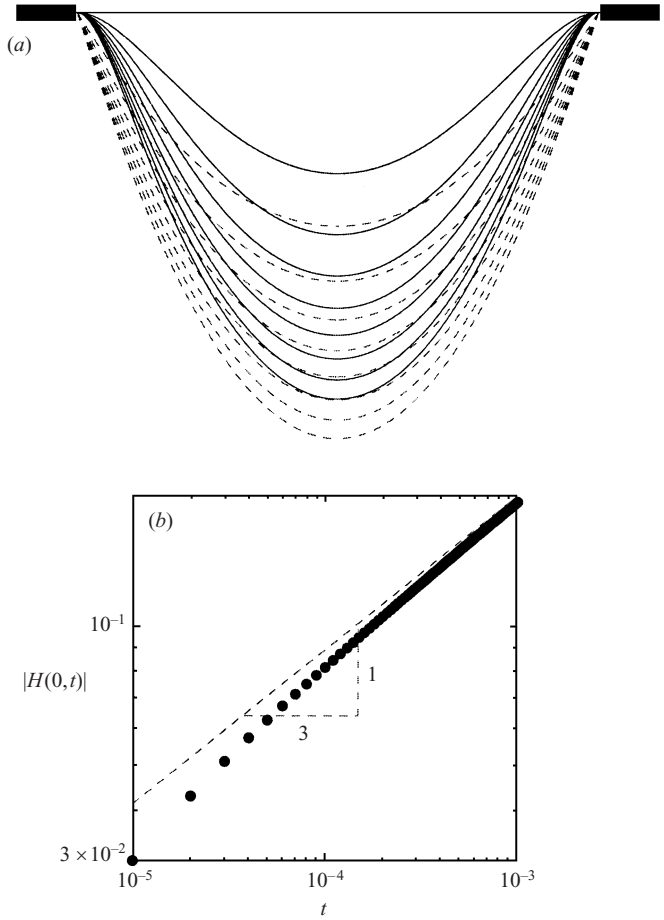

FIGURE 4. (*a*) The evolution of the filament height $H(x,t)$ at intermediate times, when the filament is dominated by stretching for the same parameter values as in figure 3. The dashed line corresponds to the stretching solution given by integrating (4.2), while the solid line represents the numerical solution to (2.16). Observe that the stretching solution does not satisfy the boundary condition $\theta(1/2) = 0$. (*b*) The maximum sag $|H(0,t)|$ vs. scaled time t in the regime dominated by stretching, determined by solving (2.16). The dashed line depicts the result obtained by balancing stretching and gravity, which yields $H \sim t^{1/3}$.

5. Late-time behaviour

As the filament continues to stretch, the changes in its cross-section can no longer be neglected, and we must solve the complete set of equations (2.1)–(2.6). However, since stretching still dominates over most of the catenary, $M \approx 0$, so that we have the simplified system of equations for the outer solution

$$T_s = w\sin\theta, \quad T\theta_s = w\cos\theta, \quad T = 3\mu A\frac{\lambda_t}{\lambda} = -3\mu A_t. \tag{5.1a–c}$$

Eliminating T from (5.1*a*) and (5.1*c*) yields $A_{st} = -w\sin\theta/3\mu$, which relation may be used in (5.1*b*) to eliminate θ leading to $A_t A_{sst} + A_{st}^2 = w^2/9\mu^2$. Integrating this last equation twice, and using the symmetry of the solution about $s = 0$ gives

$$A_t = -\left(f(t) + \frac{w^2 s^2}{9\mu^2}\right)^{1/2}. \tag{5.2}$$

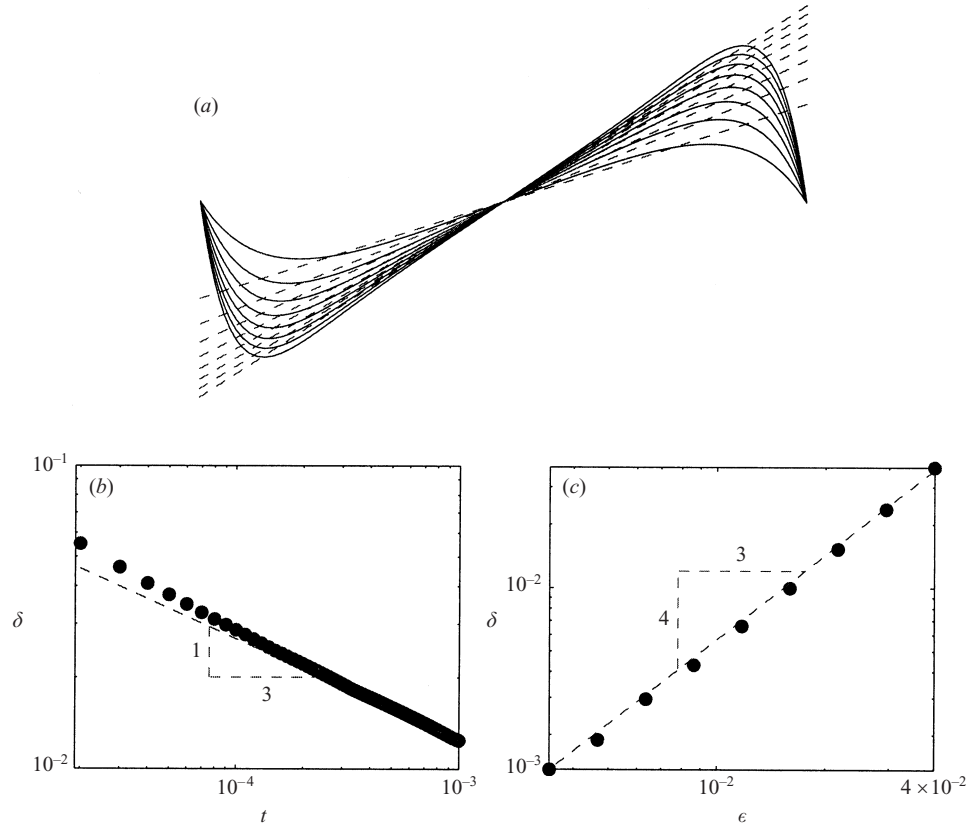

FIGURE 5. (*a*) To understand the intermediate time behaviour, we show the similarity solution to the outer problem $\theta^{(o)} \sim xt^{1/3}$ (dashed line), and the numerical solution of (2.16) for various times. The two solutions agree everywhere except near the clamped boundaries, where a dynamic bending boundary layer of width $\delta(t, \epsilon)$ persists. The dependence of δ on the scaled time t is shown in (*b*), while (*c*) shows the dependence on the aspect ratio ϵ, plotted on a log-log scale. The dashed lines show the scaling estimates (4.3) and are in accordance with the numerical solution.

Here $f(t)$ is a constant of integration that must be found by matching this outer solution to the inner bending boundary layer solution in the neighbourhood of the clamping boundaries, which can be parametrized in terms of the horizontal component of the instantaneous tension in the catenary. Since three-dimensional effects eventually become important in the ever-narrowing boundary layer, a numerical solution of the three-dimensional Stokes equations is the only resort (Stokes, Tuck & Schwartz 2000), a path we will not pursue here.

At even later times, the catenary is so thin and long as to be effectively vertical over most of its length. Then $\theta \to \pi/2$, $\theta_s \to 0$, so that $T_s = w = \rho g A_0(s)$, which when integrated leads to $T = \rho g \int_0^s A_0(s)\,\mathrm{d}s$. Substituting this expression for the tension in the constitutive equation $T(s,t) = -3\mu A_t$ and integrating yields

$$A(s,t) = -\frac{\rho g t}{3\mu} \int_0^s A_0(s)\,\mathrm{d}s + A_0(s). \tag{5.3}$$

The time and location of pinch-off are determined by setting $A(s, t^*) = 0$ in (5.3)

which gives

$$t^*(s) = \frac{3\mu A_0(s)}{\rho g \int_0^s A_0(s)}. \tag{5.4}$$

The filament will break at the (Lagrangian) position $s = s^*$ that minimizes $t^*(s)$. Since $A_t = -T(s,t)/3\mu$, the catenary will thin most rapidly in the region near the clamped boundary, where the tension is highest. Thus, in fact, $A_0(s)$ for the late-time problem will have a minimum near the wall, and the filament will break in the vicinity of the transition zone between the bending boundary layer and the stretching solution (Stokes *et al.* 2000). This process will involve shear and extensional deformations and is outside the scope of our simple slender body approximation.

Our analysis has been predicated on the assumption that inertial forces can be neglected. As the filament thins and speeds up this assumption is violated. This can be seen in the blurred image figure 1(f) of the sagging catenary. A simple estimate of the time scale when inertial effects can no longer be ignored is given by comparing the acceleration of the filament with g. Since $H \sim (\rho g/\mu L^2)^{1/3} x^2 t^{1/3}$, the maximum acceleration $H_{tt} \sim (\rho g/\mu L^2)^{1/3} L^2 t^{-5/3}$, whence $t_i \sim 1$ s, consistent with our observations. Beyond this stage, the equations of equilibrium (2.1)–(2.3) must be modified to account for inertial effects.

6. Discussion

In the history of physics, the catenary played a crucial role in elucidating the connection between shape and stress, i.e. geometry and mechanics. While its viscous counterpart cannot make such claims, it can be argued to be far richer in terms of the phenomena observed. In particular, it highlights the strong analogy between Hookean elasticity and Newtonian hydrodynamics. Atypically for a fluid, extensional deformations dominate much of the evolution of the filament, and shear deformations become important only at late times in the neighbourhood of the supporting boundaries. The separation of scales induced by the slenderness of the filament leads to a vast disparity in the time scales (and forces) associated with bending and stretching a filament. This is clearly revealed in the different rates of sagging during the initial and intermediate stages, and leads to dynamic bending boundary layers which are analogous to the folding, coiling and rippling boundary layers (Mahadevan *et al.* 1998; da Silveira *et al.* 2000; Skorobogatiy & Mahadevan 2000) in other geometries.

What remains to be done? Our approach to the problem has focused on those aspects that are amenable to the slender-body theory, and is limited to moderate deformations. When the deformations become large, a three-dimensional numerical approach to the behaviour of the filament close to the clamping boundaries is necessary to complement our simple approach outlined in § 5. As for comparison with experiments, we note that the pure bending regime is inaccessible with golden syrup at room temperatures. However, for the stretching-dominated regime, our observations are qualitatively in agreement with our predictions. Quantitative experiments to probe the validity of our theory remain an important future goal, as do extensions to include interfacial, inertial and non-Newtonian effects that could all be relevant in materials processing.

We thank J. Dumais for help with the imaging. J. T. was partially supported by an NSF graduate fellowship (1996–2001). Additional support via the US Office of Naval Research Young Investigator Program to LM (2000–03) is acknowledged.

REFERENCES

Howell, P. D. 1996 Models for thin viscous sheets. *Eur. J. Appl. Maths* **7**, 321–343.

Johnson, A. M. & Fletcher, R. C. 1994 *Folding of Viscous Layers*. Columbia, New York.

Love, A. E. H. 1944 *A Treatise on the Mathematical Theory of Elasticity*, p. 422. Dover.

Mahadevan, L., Ryu, W. & Samuel, A. 1998 Fluid rope trick investigated. *Nature* **392**, 140; and correction **403**, 502 (2000).

Rayleigh, Lord 1922 *Theory of Sound*, vol. II, p. 313. Dover.

da Silveira, R., Chaieb, S. & Mahadevan, L. 2000 Rippling instability of a collapsing bubble. *Science* **287**, 1468–1471.

Skorobogatiy, M. & Mahadevan, L. 2000 Folding of viscous filaments and sheets. *Europhys. Lett.* **52**, 532–539.

Stokes, G. G. 1845 On the theories of the internal friction of fluids in motion and of the equilibrium and motion of elastic solids. *Trans. Camb. Phil. Soc.* **8**, 287–347.

Stokes, Y. M., Tuck, E. O. & Schwartz, L. W. 2000 Extensional fall of a very viscous fluid drop. *Q. J. Mech. Appl. Maths* **53**, 565–582.

Taylor, G. I. 1969 Instability of jets, threads and sheets of viscous fluid. *Proc. 12th Intl Conf. on Applied Mechanics*, pp. 382–389.

Trouton, F. T. 1906 On the coefficient of viscous traction and its relation to that of viscosity. *Proc. R. Soc. Lond.* A **77**, 426–440.